Time-resolved spectroscopy of self-trapped excitons in fluorite crystals

R. T. Williams and M. N. Kabler
Naval Research Laboratory, Washington, D. C. 20375

W. Hayes and J. P. Stott
Clarendon Laboratory, Oxford University, Oxford, England

(Received 3 February 1976)

We report time-resolved measurements of optical emission and absorption in crystals of CaF_2, SrF_2, and BaF_2 following excitation by pulsed ionizing radiation. Prominent transient absorption bands in the visible and ultraviolet are observed, and their decay is resolved into several time components which correspond to those of the emission. The absorption is shown to originate in the same excited electronic states as the intrinsic recombination luminescence. These states have been identified previously as self-trapped excitons, largely on the basis of polarization measurements and optically detected EPR in the excited states. These results, augmented by kinetic data from the present experiments and by new polarization data, suggest a fairly detailed picture of the various localized electronic states involved in the process of electron-hole recombination in fluorites. The ionic relaxation associated with the self-trapped exciton is evidently more complex than in, e.g., the alkali halides; in the fluorites the lowest triplet states of the self-trapped exciton have been found to resemble a metastable nearest-neighbor fluoride vacancy-interstitial pair, i.e., an F-H-center pair, with probable point symmetry C_{1h}.

I. INTRODUCTION

Pure fluorite crystals luminesce strongly under band-gap excitation. In CaF_2, SrF_2, and BaF_2, the intrinsic emission comprises a broad band with peak near 300 nm.[1] The extraordinarily large Stokes shift, about 7 eV between the first exciton absorption peak and the intrinsic emission-band peak, is suggestive of the phenomenon of exciton self-trapping, which is well known in alkali halides.[2] Indeed, self-trapping of holes in the fluorite crystals has long been established by EPR and optical methods.[3] The self-trapped hole, or V_k center, comprises a hole localized on two adjacent halide ions thereby bound to each other in an X_2^- molecular configuration. The initial association of the intrinsic emission in fluorites with recombination of electrons and self-trapped holes was achieved by a measurement of polarization similar to that first employed in alkali halides. In crystals doped with thulium to provide electron traps, self-trapped holes were created by irradiation and aligned by polarized optical bleaching. The luminescence produced upon annihilation of the aligned V_k centers with electrons photoexcited from the traps was found to match satisfactorily the spectrum of x-ray-excited intrinsic emission and to be polarized along the V_k alignment direction.[1] A related experiment in which the electrons were photoexcited from traps by a short pulse of light indicated that the decay of the resulting luminescence involves a component with lifetime $\tau < 40$ nsec at low temperature.[1] No other measurements of the luminescence decay time appear to have been made.

Recently, the technique of optical detection of electron paramagnetic resonance in the excited states responsible for intrinsic luminescence has been applied to the alkaline-earth fluorides.[4] The data show the existence of a light-emitting triplet state of the self-trapped exciton (STE) and further indicate that the intrinsic emission has decay-time components with $\tau \gg 40$ nsec. In fact, the variation of the EPR signal with microwave chopping frequency can be interpreted to indicate a component with $\tau \approx 10$ msec in CaF_2 at 1.6 K.[5] Further aspects of the EPR experiments, particularly the symmetry properties of the spin Hamiltonian, will be discussed in relation to results being reported in this paper.

Thus the identification of intrinsic emission with STE's in the fluorite crystals is well established. If metastable STE levels are populated to a significant degree by irradiation, we may expect transient excited-state absorption spectra to be exhibited, as they are in the alkali halides.[6,7] In this connection, we note that Patterson and Fuller measured absorption produced by pulsed-electron irradiation of CaF_2 at room temperature.[8] However, no attempt to relate the transient absorption to luminescence properties of the crystal was reported. It is known that x-ray or particle irradiation at low temperature produces stable F centers and complementary interstitial fluorine atoms or ions, although at somewhat lower efficiency than that of the corresponding processes in alkali halides.[9] These defects might

be expected to appear also in transient optical spectra under favorable circumstances. It is notable that, in the alkali halides, the STE is known to play the role of an intermediate state in the photochemical process which produces F centers.[10]

In the present paper, we describe measurements of the time dependence of optical emission and absorption in crystals of CaF_2, SrF_2, and BaF_2 following excitation by a pulse of energetic electrons. These results suggest a fairly detailed picture of the various localized electronic states involved in the process of electron-hole recombination.

II. EXPERIMENT

The experimental apparatus is basically the same as employed in earlier spectroscopy of self-trapped excitons in alkali halides.[6,7,11] Electron pulses of 5-nsec duration and 500-keV mean electron energy were used to excite the crystals. The rotating-mirror arrangement used for fast spectral scans in Ref. 7 was replaced in the present investigation by a silicon-target vidicon having extended uv response (RCA type C23231). Photomultipliers having S-20 or S-1 photocathode surfaces and 2-nsec anode pulse rise times were employed to measure time dependence of emission and absorption at fixed wavelengths. The oscilloscope used for recording fast signals had a 250-MHz bandwidth.

Light sources used for absorption spectroscopy included a dc xenon arc lamp and a 50-J (input energy) xenon flashlamp having a pulse duration of 25 μsec full width at half-maximum. Absorption spectra were recorded at specific times by delaying the lamp flash with respect to the electron pulse. The pulse duration of the flashlamp is considered negligible for spectra recorded at times 0.5 msec or longer after the electron pulse. When we have occasion to refer to spectra measured after a delay of 20 μsec, however, it is meant that the peak intensity of the lamp flash occurs at 20 μsec after the electron pulse. In fact the absorption spectrum is integrated from about 5 to 40 μsec in this case. A combination of color filters and a contoured aperture in the image plane of the spectrograph was employed to attenuate the brightest portions of the xenon spectrum, in order to avoid exceeding the dynamic range of the detection apparatus at any point of the spectrum. The high intensity of the flashlamp enabled us to discriminate effectively against the very intense intrinsic luminescence, whereas practical use of the dc xenon arc in making fixed-wavelength measurements of absorption was limited to wavelengths away from the peak of the luminescence.

Undoped alkaline-earth fluoride crystals were obtained from Harshaw Chemical Co. Radiolysis of crystals from this source has been studied previously.[1,9] Samples were cut and polished in a rectangular shape about $8\times8\times2$ mm^3, to take advantage of the internal-reflection geometry used to increase the optical path length through the electron-penetration layer.[11]

For measuring temperature dependence of the emission decay times, crystal excitation was accomplished with a 5-nsec pulse of x rays obtained by directing the 500-keV electrons onto a tungsten target. The energy density deposited in the sample by a single x-ray pulse was less than 1 μJ/cm^3, so heating of the sample was negligible even at the lowest temperatures. For measurements at 4.2 and 1.8 K, the crystal sample was immersed in liquid helium. For measurements of emission decay times between 10 and 300 K, the sample was mounted with heat-sink compound on the cold finger of a variable-temperature cryostat, with a thermocouple and germanium resistance thermometer attached to the cold finger.

Measurement of transient absorption required the more intense excitation available by use of the electron pulse directly, with typically 4 mJ/cm^2 incident on the sample. Measurements were made at three temperatures with the crystal mounted on the cold finger of a simple cryostat. Heating of the sample by the electron pulse was negligible at room temperature and liquid-nitrogen temperature. With liquid helium in the cryostat reservoir, the effective sample temperature shortly after an electron pulse was estimated to be about 10 K. Emission measurements were made under these same conditions to facilitate comparison to the absorption data.

III. RESULTS

A. Luminescence components at 10 K

In Figs. 1 and 2 we display the decay characteristics of the intrinsic emission-band peaks in CaF_2 and SrF_2 at $T=10$ K. In order to accommodate the data (spanning six decades in time) on a semilogarithmic plot we have inserted two expanded time scales in each figure. In the emission data for both crystals, a fast decay component with $\tau\approx10$ nsec is easily distinguished. Inspection of the decay at longer times readily shows that at least three additional components are involved. In order to determine whether a sum of four exponentials is sufficient as well as necessary to fit the complete decay curve, we

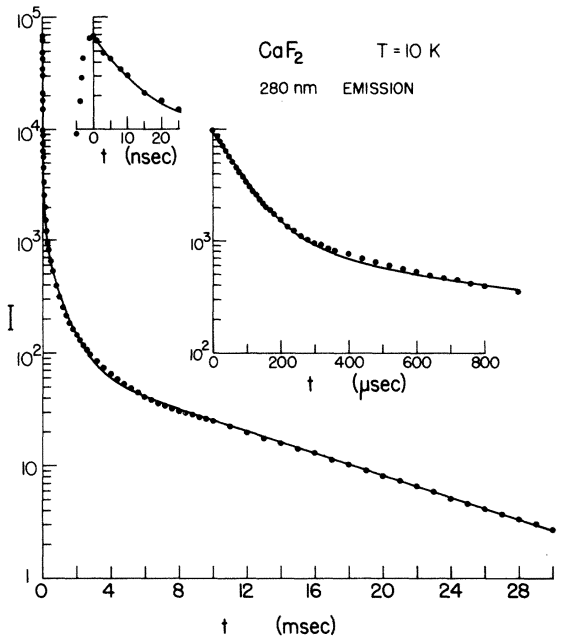

FIG. 1. Decay of 280-nm emission in CaF_2 at $T = 10$K is plotted on three time scales, with a common intensity scale. The lines represent a best-fit sum of four exponentials [Eq. (1)], with the parameters listed in Table I.

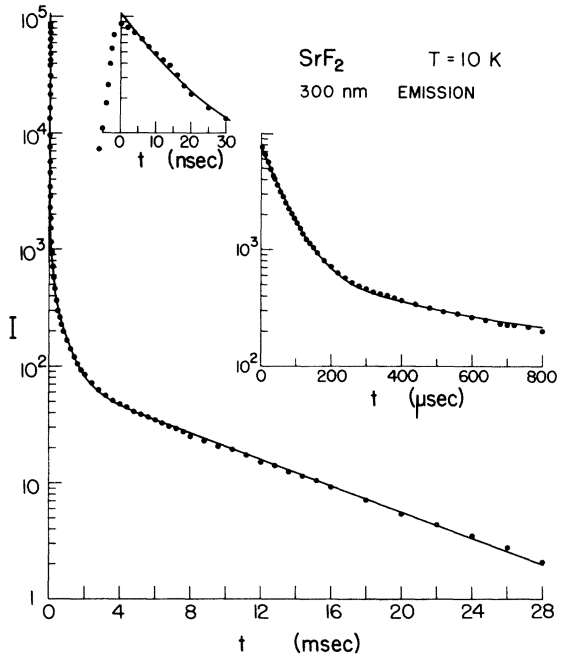

FIG. 2. Decay of 300-nm emission in SrF_2 at $T = 10$ K is plotted on three time scales, with a common intensity scale. The lines represent a best-fit sum of four exponentials [Eq. (1)], with the parameters listed in Table I.

have computed the variational best fits, which are shown as lines in Figs. 1 and 2. Agreement is within experimental uncertainty. Note that three of the four exponential decay components in each data set are readily distinguishable by inspection since they are well separated in time.

The parameters required to fit the decay of emission (at the band peak) in CaF_2, SrF_2, and BaF_2 at $T = 10$ K are listed in Table I. For each crystal, the first row of parameters lists the time constants τ_i which appear in the fitted expression for emission intensity

$$I(t) = \sum_i A_i e^{-t/\tau_i}, \tag{1}$$

while the second row of parameters lists the corresponding preexponential factors A_i. The factors A_i were normalized such that $I(0) = 1$. As noted above, four exponentials appear to be necessary and sufficient to fit the data for CaF_2 and SrF_2 within experimental error; however a fifth term is necessary to achieve a comparable fit for BaF_2.

It is readily apparent that most of the *peak intensity* under pulse excitation, e.g., about 90% in SrF_2, is associated with the 10-nsec component. This is consistent with the finding by Beaumont *et al.* of a single component with $\tau < 40$ nsec.[1] They used photoexcitation of trapped electrons by a flashlamp to promote electron-hole recombination on a pulse basis, and the luminescent intensity was evidently too low to allow detection of long-lived components. Table I also displays parameters characterizing the integrated intensity at the band peak:

$$S(t) = \int_t^\infty I(t)\, dt = \sum_i A_i \tau_i e^{-t/\tau_i}. \tag{2}$$

The light sum $S(0)$ is normalized to unity in the table presentation. Inspection of the coefficients $A_i \tau_i$ demonstrates that the 10-nsec component accounts for an almost negligible fraction of the *total emission* at these wavelengths. We also note that the three longer-lived components are roughly equal in integrated intensity both in CaF_2 and SrF_2, and that the four longer-lived components in BaF_2 are roughly comparable to each other. The long-lived components account for >99% of the emission intensity at these wavelengths in steady state.

The spectra of steady-state x-ray-excited emission in pure CaF_2, SrF_2, and BaF_2 at 77 K were presented in Ref. 1. Recent measurements[5] of the x-ray-excited emission spectra at temperatures down to 1.6 K showed that there is little change in the band shape at temperatures lower

TABLE I. Parameters obtained by fitting Eqs. (1)–(3) to the decay of emission and absorption at $T = 10$ K.

	i	1	2	3	4	5
CaF_2	τ_i	10 nsec	83 μsec	870 μsec	8.8 msec	∞
280-nm emission	A_i	0.84	0.14	0.014	0.0013	•••
$S(0)$	$A_i\tau_i$	0.000 24	0.33	0.34	0.33	•••
450-nm absorption	D_i	•••	0.48	0.31	0.20	~0.01
SrF_2	τ_i	11 nsec	59 μsec	640 μsec	7.7 msec	∞
300-nm emission	A_i	0.93	0.068	0.0050	0.000 74	•••
$S(0)$	$A_i\tau_i$	0.000 80	0.31	0.25	0.44	•••
515-nm absorption	D_i	•••	0.32	0.42	0.25	~0.01
BaF_2	τ_i	12 nsec	53 μsec	710 μsec	5.4 msec	29 msec
310-nm emission	A_i	0.90	0.089	0.015	0.000 41	0.000 071
$S(0)$	$A_i\tau_i$	0.000 55	0.24	0.54	0.11	0.10

than 77 K. The emission bands in all three crystals are somewhat asymmetric, with extended long-wavelength tails. In view of the multiple decay components we have found at the peak of each emission band, it is essential to determine whether the entire band decays uniformly or whether there is a spectral variation of the decay characteristics.

In the upper portion of Fig. 3, we have reproduced (in solid lines) the emission spectra for SrF_2 and CaF_2 from Ref. 1 to represent the low-temperature, steady-state band shapes. The spectral distribution of each 10-nsec emission component, as determined in the present experiments, is shown by the broken line. This component clearly does not coincide with the steady-state band, which corresponds to the time-integrated sum of all decay-time components [Eq. (2)]. The 10-nsec component contributes to the asymmetry of the overall band, but cannot account for all of the asymmetry since it comprises less than 1% of the total emission.

Determination of the spectrum of the 10-nsec component was straightforward, because its decay time is about 3 orders of magnitude different from those of the other emission components. To separate the three slower components spectrally, we have generated variational best fits, similar to those in Figs. 1 and 2, at five wavelengths across the emission bands in SrF_2 and CaF_2. First, the optimum values of τ_i and A_i at the band peak were determined, as listed in Table I. Thereafter, in fitting the data at the four remaining wavelengths, only the preexponential factors A_i were varied. The time constants τ_i were assigned values corresponding to those at the band peak. Thus the value $A_i\,\tau_i$ as a function of wavelength represents the contribution of the τ_i component to the time-integrated emission at the given wavelength. This is represented graphically in the lower portion of Fig. 3, where the normalization corresponds to $\sum A_i\,\tau_i = 1$, as discussed following Eq. (2). Note that the values of $A_i\,\tau_i$ for the 10-nsec component (solid points) are displayed on a $\times 10$ scale. We have used open squares, triangles, and circles, respectively, to correspond to the other three τ_i values in Table I, in order of increasing τ_i.

Inspection of the spectral variation of the $A_i\,\tau_i$ values in SrF_2 indicates rather clearly that the long-wavelength side of the emission band is dom-

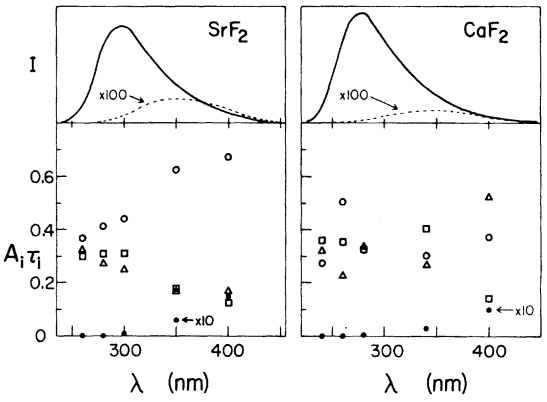

FIG. 3. Solid lines in the upper part of the figure represent the luminescence bands excited by continuous x irradiation of SrF_2 and CaF_2 at $T = 77$ K (from Ref. 1). The broken lines show the approximate band shape, on a $\times 100$ expanded scale, of the ~ 10-nsec component of emission measured in this experiment at $T = 10$ K. The lower part of the figure presents the quantities $A_i\,\tau_i$ [see Eq. (2)] obtained by fitting the luminescence decay to a function of the form of Eq. (1), at several wavelengths. The identification of the point symbols with the decay times in Table I is as follows: (●, 1); (□, 2); (△, 3); (○, 4). Component 1 (●) is displayed on a $\times 10$ expanded scale.

inated by the slow component. The 400-nm point may be affected by other components which become discernible in the band tail, but these are far too weak to affect the analysis at other wavelengths. That is, at all points except 400 nm, the fits to the assigned values of τ_i were comparable in quality to the fit at the band peak, indicating that the band is principally composed of the three slower components being considered.

The corresponding spectral decomposition for CaF_2 in the lower right portion of Fig. 3 does not indicate a clear trend, and certainly does not indicate domination of the long-wavelength side of the band by the slow component. Here again, weak components with $\tau \approx 2.4$ msec and 3 μsec show up in the extreme tails of the band, but the three principal components used in fitting appear to account adequately for about 95% of the total emission.

B. Absorption components at 10 K

Absorption spectra measured at several delay times after electron-pulse excitation are shown in Figs. 4–6, for CaF_2, SrF_2, and BaF_2 at $T = 10$ K. These data were obtained by recording the transmitted spectrum of the 25-μsec xenon lamp flash with a silicon-target vidicon. The estimated uncertainty limits are indicated in the figures. In some parts of the spectra, the resolution is better than indicated. For example, we are confident after repeated measurements that the structure in the low-energy band of SrF_2 is real. On the other hand, the jaggedness of the ultraviolet portions of all spectra is noise consequent to the lower light intensity available there and does not represent real structure in the absorption spectrum.

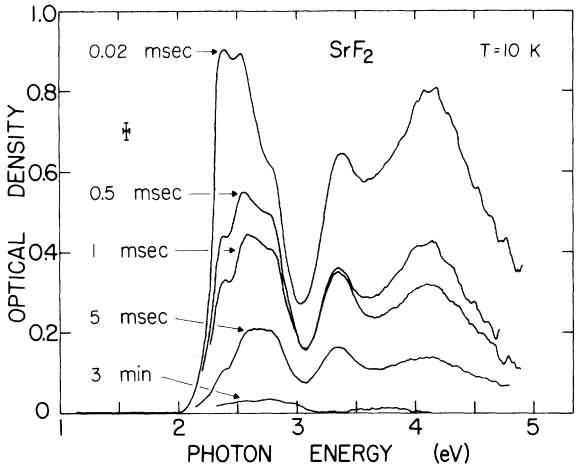

FIG. 5. Optical absorption in SrF_2 ($T = 10$ K) is shown for the indicated delays after irradiation by a pulse of energetic electrons. Instrumental resolution is indicated in the figure.

Addressing first the CaF_2 spectra in Fig. 4, we may compare the major spectral features with peak energies of known color-center bands. The F band in CaF_2 occurs at 3.3 eV,[12] which actually corresponds to a minimum in the transient absorption spectrum. The H and V_k bands, which are the strongest absorptions of the interstitial F atom and self-trapped hole, have peaks at approximately 4 and 3.88 eV, respectively, in CaF_2.[1,13] Although the broad transient ultraviolet absorption bears some resemblance to an H or V_k band, it occurs at somewhat higher energy.

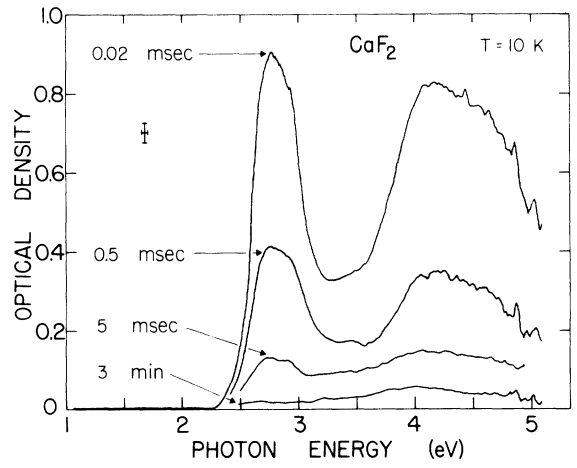

FIG. 4. Optical absorption in CaF_2 ($T = 10$ K) is shown for the indicated delays after irradiation by a pulse of energetic electrons. Instrumental resolution is indicated in the figure.

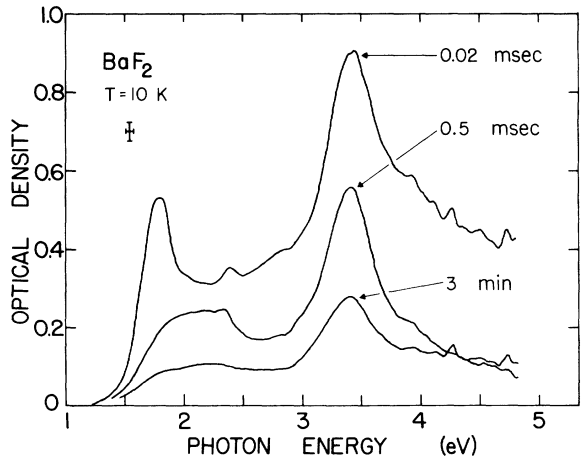

FIG. 6. Optical absorption in BaF_2 ($T = 10$ K) is shown for the indicated delays after irradiation by a pulse of energetic electrons. Instumental resolution is indicated in the figure.

Both of the major features in the transient absorption spectrum decay at approximately the same rate, leaving only a small stable absorption continuum. The magnitude of the stable (3 min) absorption shown corresponds approximately to that produced by the first pulse of electrons incident upon a given sample. On subsequent irradiation pulses, in the absence of bleaching, very little additional *permanent* absorption was produced. That is, the growth of permanent absorption saturates, but the transient spectrum does not change noticeably after repeated irradiation.

In SrF_2 (Fig. 5) the absorption spectrum exhibits more structure, and does not decay uniformly in time. The two major bands resemble those found in CaF_2. The principle low-energy band is at somewhat lower energy than the 2.85-eV peak of the F band in SrF_2. The main ultraviolet band is at somewhat higher energy than the H and V_k peaks, which would occur at approximately 4 and 3.80 eV, respectively.[1,13] The 3.35-eV transient band decays, along with one component of the low-energy absorption, in a time of the order of 10 msec.

Though less evident, several features of the transient absorption spectra in BaF_2 (Fig. 6) also resemble the CaF_2 and SrF_2 spectra. If the 0.5-msec absorption spectrum is subtracted from the 0.02-msec spectrum, the resulting difference spectrum is virtually free of the 3.4-eV peak and exhibits the general two-band pattern characteristic of CaF_2 and SrF_2. The "red" transient band occurs just to the low-energy side of the F-band peak ($E_F = 2.03$ eV), and the principal ultraviolet band in the difference spectrum has its peak at roughly 4 eV. The residual (3 min) absorption spectrum including the 3.4-eV peak resembles the bands reported by Cavenett *et al.* following x irradiation of undoped BaF_2 at 77 K.[14] The residual absorption saturates after a few electron pulses, and can be optically bleached.

The efficiency of converting electron-pulse input energy into transient absorbing species in these alkaline-earth fluoride crystals is quite comparable to the efficiency of creating self-trapped excitons in alkali halides, if we assume comparable oscillator strengths for the major bands.

Before discussing other features of the spectra, let us consider in more detail the decay of absorption at specific wavelengths. Figure 7(a) presents the time dependence of absorption at 2.76 eV (450 nm) in CaF_2 at $T = 10$ K. The curve is again a least-squares fit to a sum of exponentials [analogous to Eq. (1)], but in this case *only* the preexponential factors D_i in the fitting function

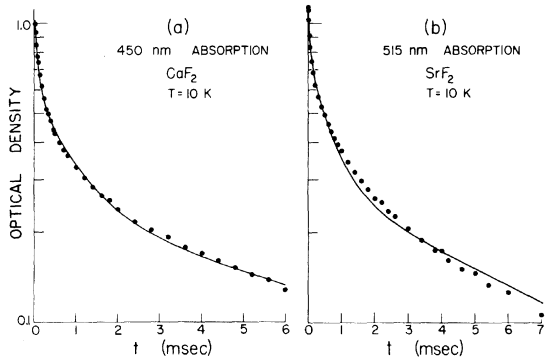

FIG. 7. Decay of 450-nm absorption in CaF_2 (a) and 515-nm absorption in SrF_2 (b) at $T = 10$ K is represented by points. The lines represent best fits to functions of the form of Eq. (3), where the parameters τ_i are fixed at the values in Table I determined from analysis of luminescence decay. Values of the free parameters D_i determined by fitting the absorption decay are listed in Table I.

$$D(t) = \sum_i D_i e^{-t/\tau_i} \tag{3}$$

are varied as fitting parameters. The time constants τ_i are taken from analysis of the emission data in Fig. 1, although an additional term with $\tau_5 = \infty$ is required in the fitting function to take account of the weak permanent absorption. The fitting parameters are given in Table I.

The motivation for this kind of analysis comes from the hypothesis that the absorption and emission arise from the same set of initial levels. The integrated intensity function $S(t)$ defined in Eq. (2) represents the sum of light which will be emitted after time t, but it is also, under certain circumstances, a sum of terms proportional to the populations of the emitting levels at time t. Those circumstances are that the intensity we measure be proportional to the total emission in the band in question, and that there be no competing nonradiative decay channels. Optical absorption which originates in the emitting levels can be represented by a sum of exponentials with the same time constants that govern emission (including $\tau = \infty$). The terms will be proportional to the populations of the contributing levels under conditions very similar to those on emission; namely, that the spectra and oscillator strengths for absorption originating in each of the contributing levels be identical.

Despite these fairly stringent requirements on both emission and absorption, comparison of the parameters for absorption and for integrated emission in CaF_2 (Table I) shows reasonable agreement. Recalling in addition that the absorption data were fit with predetermined time

constants, we conclude that the absorption at 450 nm and the intrinsic emission in CaF_2 originate from the same electronic state. Data for $T = 77$ K to be presented later provide more evidence for this conclusion.

The decay of 2.4-eV (515 nm) absorption in SrF_2 at 10 K is shown in Fig. 7(b). The line is the best fit obtainable with fixed time constants determined from the emission (Fig. 2). It lies somewhat outside the limits of our estimated experimental uncertainty, suggesting that the absorption includes a component not related directly to the emitting levels. If the fitting function is allowed to contain one additional exponential term, with $\tau = 1.4$ msec, good agreement is obtained. There is approximate agreement between the fitting parameters for absorption and the integrated emission in Table I, again suggesting common states of origin for emission and most of the absorption. Indeed, we should not expect exact agreement of the preexponential fitting parameters in the case of SrF_2, since Figs. 3 and 5 show that neither the emission nor the absorption spectra for different decay-time components are identical.

To further examine the spectral decomposition of the decay-time components in absorption, consider Fig. 8. The energy range represented corresponds to the major low-energy absorption bands in SrF_2 and CaF_2. In the figure we represent the difference ΔD between absorption spectra measured at selected times. The times were chosen to bracket portions of the decay curve in which only one time constant is dominant. Thus the chain curve for SrF_2 in Fig. 8 is the difference in absorption between 20 and 80 μsec and should represent the approximate band shape of the 59-μsec component. The solid curve is the difference between spectra measured at 0.5 and 1 msec, roughly representing the 640-μsec component. The 7.7-msec component corresponds approximately to the dashed curve, which is the difference in spectra measured at 5 and 10 msec. The same set of times is represented for CaF_2, except that the chain curve is the difference between spectra at 20 and 100 μsec.

C. Luminescence and absorption at 77 K

The decay of 280-nm emission in CaF_2 at a temperature of 77 K is shown in Fig. 9. The 10-nsec component is virtually unchanged from low temperature. However, the subsequent decay is now described by one exponential with $\tau = 57$ μsec, instead of the three required at 10 K. This behavior suggests that approximate thermal equilibrium obtains among the emitting levels at 77 K.

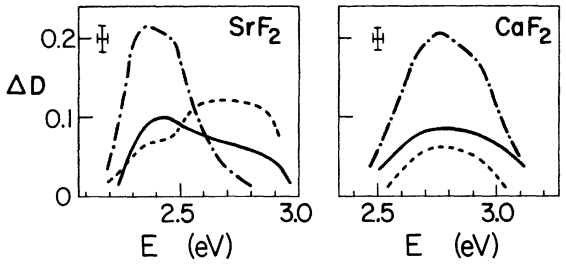

FIG. 8. Each spectrum is the difference (ΔD) between absorption spectra measured at two different delays after pulsed-electron irradiation at $T = 10$ K. The chain curve corresponds to D(20 μsec) − D(80 μsec) for SrF_2, and to D(20 μsec) − D(100 μsec) for CaF_2. For both crystals, the solid curve represents D(0.5 msec) − D(1 msec) and the broken curve represents D(5 msec) − D(10 msec).

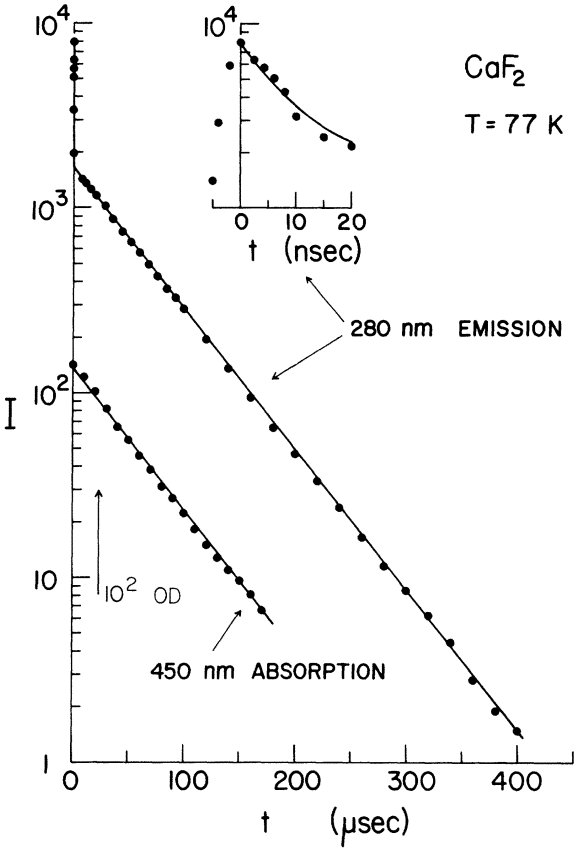

FIG. 9. Decay of 280-nm emission in CaF_2 at $T = 77$ K is plotted on two time scales, with a common intensity scale. The lines represent a best-fit sum of two exponentials, as in Eq. (1). In the lower left, the decay of 450-nm absorption at 77 K is shown as 10^2 OD, where OD is the measured optical density. The slope of the line is the same as for the 57-μsec component of emission.

The decay of 450-nm absorption in CaF_2 at 77 K is shown in the lower portion of Fig. 9. The slope of the line drawn through the absorption data was determined from the emission data. This again demonstrates the connection between absorption and emission.

As shown in Fig. 10, the 300-nm emission in SrF_2 at 77 K has two decay components in addition to the 10-nsec component. The 515-nm absorption data in Fig. 10 can be fit adequately by a sum of two exponentials with time constants determined from the emission, and a third with $\tau = \infty$. If we represent the absorption, emission, and time-integrated emission in the form

$$\sum_i A(\tau_i) e^{-t/\tau_i}, \tag{4}$$

i.e., labeling the coefficients A by the corresponding time constants, the ratio $A(20\ \mu\text{sec})/A(180\ \mu\text{sec})$ in absorption is 18. The corresponding ratio of coefficients in the representation of emission intensity is 16, in good agreement. On the other hand, the ratio of corresponding parameters in the time-integrated emission $[S(t)]$ is 1.8, in significant disagreement. This is understandable if one level having decay time $\tau = 20\ \mu$sec both absorbs and emits light, while being fed by a separate level ($\tau = 180\ \mu$sec) which neither absorbs nor emits in the spectral regions monitored. According to this interpretation, the level (or set of levels in equilibrium) from which the 300-nm emission and 515-nm absorption in SrF_2 originate has a single exponential decay with $\tau = 20\ \mu$sec at 77 K. The essential change upon warming from 10 to 77 K thus appears to be analogous to the case of CaF_2, i.e., the collapse of three components to one.

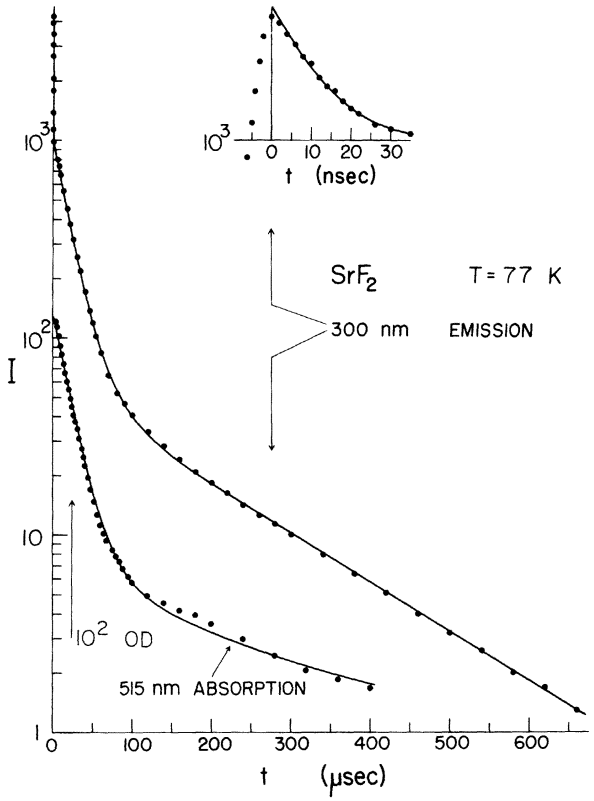

FIG. 10. Decay of 300-nm emission in SrF_2 at $T = 77$ K is plotted on two time scales, with a common intensity scale. The lines represent a best-fit sum of three exponentials, as in Eq. (1). In the lower left, the decay of 515-nm absorption at 77 K is plotted as 10^2 OD, where OD is the measured optical density, and fitted to a sum of two exponential-decay components with time constants fixed at the values determined for the longer two components of emission, and a third component with $\tau = \infty$.

D. Temperature dependence of the luminescence decay

The decay of 280-nm luminescence in CaF_2 has been measured at various temperatures between 1.8 and 300 K. After fitting the data to a sum of three or fewer exponential components as in Eq. (1) (neglecting the 10-nsec component), the best-fit values of τ_i are plotted vs temperature in Fig. 11. The *areas* of the point indicators in Fig. 11 are proportional to the products $A_i \tau_i$ [where $\sum_i A_i \tau_i = 1$; see Eq. (2)], in order to indicate the transfer of integrated emission intensity from one component to another. Similar data for SrF_2 in the temperature range 10–300 K are shown in Fig. 12.

At a temperature of 300 K, the 10-nsec component of emission is no longer evident. The 280-nm emission in CaF_2 at room temperature exhibits a principal decay time of 1.7 μsec, which accounts for 97% of the time-integrated intensity. Subsequent decay is characterized approximately by a time constant of 34 μsec. The 450-nm absorption can be fit satisfactorily with these same time constants. About 92% of the absorption at 450 nm decays with the 1.7-μsec time constant. The 300-nm emission and 515-nm absorption in SrF_2 at room temperature are characterized by a principal decay time of 2.5 μsec.

IV. DISCUSSION

A. Nature of the optical transitions

It is evident that at least a major portion of the transient absorption spectra, Figs. 4–6, arises from metastable, localized electron-hole pair states. The temporal correlations between absorption and emission spectra are the primary bases for this conclusion, since the emission

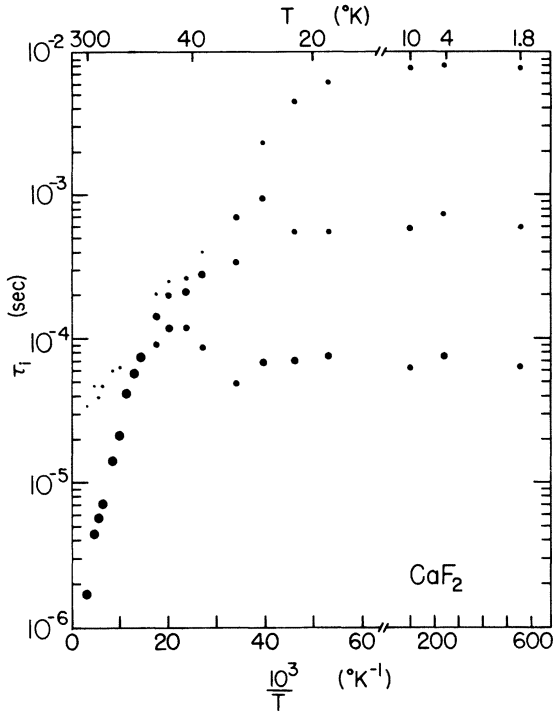

FIG. 11. Decay of 280-nm emission in CaF_2 at various temperatures has been fitted to a function of the form of Eq. (1). The time constants τ_i so determined are plotted here as a function of temperature. The area of each point indicator for τ_i is proportional to the time-integrated intensity of that component, $A_i\tau_i$ [see Eq. (2)], where $\sum_i A_i\tau_i = 1$ at a given temperature.

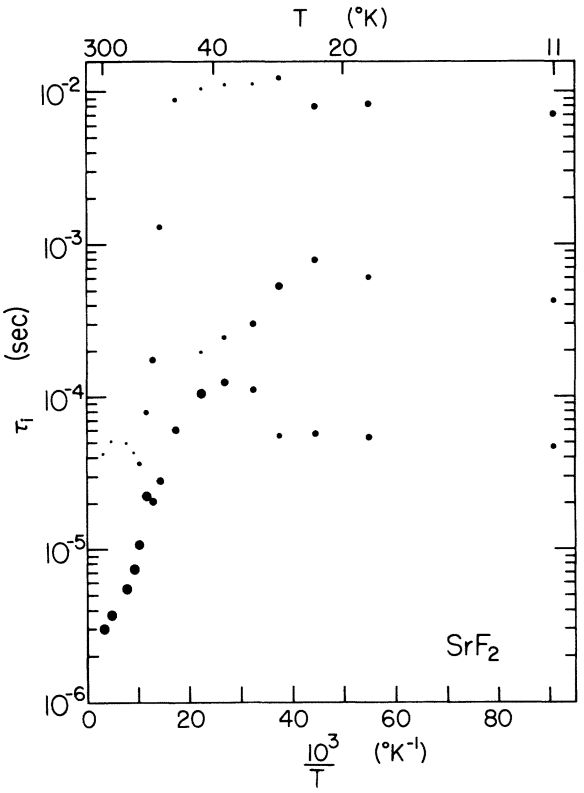

FIG. 12. Decay of 300-nm emission in SrF_2 at various temperatures has been fitted to a function of the form of Eq. (1). The time constants τ_i so determined are plotted here as a function of temperature. The area of each point indicator for τ_i is proportional to the time-integrated intensity of that component, $A_i\tau_i$ [see Eq. (2)], where $\sum_i A_i\tau_i = 1$ at a given temperature.

itself was previously shown to result, at least in large part, from the recombination of electrons and self-trapped holes. It is difficult to produce direct evidence that rules out any influence of chemical impurities on the luminescent states. Nevertheless we feel the balance of evidence indicates that these trapped exciton effects are basically intrinsic. Neither specific impurity effects nor an underlying variability in properties are apparent in the EPR data for self-trapped holes[3] or for STE's[4]; furthermore, self-trapping is an accepted phenomenon in halide lattices and is certainly not unexpected in the fluorites. Arguing from another viewpoint, since the holes are immobile at low temperatures, they are unable to seek out the 10^{-4} mole% or lower concentration of residual impurities, and thus the rates of production of extrinsic recombination sites required to account for our observed transient phenomena cannot be attained. We thus shall adopt the hypothesis that intrinsic self-trapping is the sole source of these phenomena. However, in a later section we shall discuss an effect involving the luminescence polarization which does apparently arise from impurities.

It is useful to compare the present transient absorption spectra with those previously obtained from a number of alkali chlorides, bromides, and iodides under experimental conditions similar to those for the data of Figs. 4–6.[7] The similarities between the alkali-halide and fluorite spectra are striking and strongly suggest a common origin. It has been established that triplet states of the STE are the source of the spectra in alkali halides, the STE in this case being an electron trapped at a normal X_2^- molecular ion or V_k center with no other lattice defect involved. However, for the fluorites, recent EPR measurements using optical (luminescence) detection have shown that more complex morphologies are involved, in particular a configuration wherein one of the ions in the F_2^- core is an interstitial.[4] Ignoring this difference for the moment, let us compare the fluorite and alkali-halide results in more detail.

The decay times for the primary fluorite transitions are much longer than one would expect for allowed singlet-singlet transitions, and therefore the metastable states are almost surely triplets as in the alkali halides. Comparing first the emission bands, one notes that the peak energies, measured as fractions of the respective band gaps, are roughly the same for CaF_2, SrF_2, BaF_2, KCl, KBr, KI, RbCl, RbBr, and RbI. That is, the relative Stokes shifts for these crystals are comparable. The sodium halides appear to be a special case, as discussed in Ref. 7.

Regarding triplet-state optical absorption, the characteristic spectrum in alkali halides is dominated by two broad bands: an ultraviolet band at slightly higher energy than the V_k absorption band and another band typically at somewhat lower energy than the F band. The absorption falls rapidly to zero at still lower energy. These general features are seen to be dominant also in the present spectra. Employing previous arguments[6,7] regarding the nature of these principal transitions, it is reasonable to attribute the ultraviolet absorption to a hole transition within the F_2^- core analogous to the strong $^2\Sigma_g^+ - {}^2\Sigma_u^+$ transition of the self-trapped hole. The visible band is likewise attributed to a Rydberg sequence of electron transitions similar to the lower-energy transitions of the F center. Although in the complex fluorite STE morphologies which we shall consider presently the electron is held primarily by the Coulomb field of an incipient vacancy rather than the hole itself, this difference should not affect the present qualitative comparisons. In Fig. 13, which demonstrates correlations among various absorption transitions, the approximate peak energies of the two principal transient bands and, for comparison, the transitions of stable color centers (F, V_k, and H bands) are plotted as functions of the lattice constant. As a general rule for halide crystals of a given structure, the energies of electron transitions are found to vary substantially with lattice parameter while the energies of hole transitions vary only slightly. The hole transitions are effectively screened from the lattice by virtue of their localization on the F_2^- molecular subunit. Our assignments for the transient bands are seen to fit this rule and, furthermore, the peak energies are actually rather near those of the appropriate color-center counterparts.

It is reasonable to locate the terminus of the electron Rydberg sequence at the prominent minimum in the spectra. In this manner an estimate for the optical binding energy of the trapped-exciton configuration may be obtained, as was done previously for the alkali halides.[7] For CaF_2, SrF_2, and BaF_2 these binding energies appear to be roughly 3.3, 2.9, and 2.1 eV, respectively, measured with respect to the lowest triplet state of the STE. Because of local relaxation these values are substantially larger than binding energies inferred from fundamental ultraviolet spectra, which are characteristic of a free exciton in the unrelaxed lattice. This situation is discussed in Ref. 7.

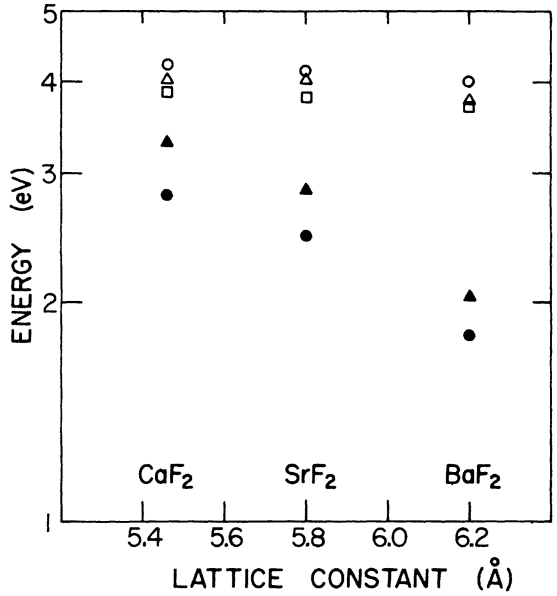

FIG. 13. Dependence on lattice constant of the peak energies of the transient low-energy absorption band (●) and the transient uv absorption band (○) is compared with the dependence of the peaks of the stable color-center bands F(▲), H(△), and V_k(□).

B. Correlation with EPR data

Data from the recent microwave-optical double-resonance experiments[4] are the key to further progress in understanding STE states in the fluorites. In order to proceed, let us deal with a preliminary question, namely, which decay-time component or components are to be associated with the observed EPR signals.

The triplet-state EPR was detected by observing changes in the intensity and/or polarization of recombination luminescence excited with steady x-ray excitation. In this type of experiment the probability of detecting a given microwave transition is greater the larger the difference between initial and final triplet sublevel populations and the longer the lifetime of the initial sublevel. Thus, in general, the longest-lived sublevel which originates luminescence is the one most likely to originate detectable double resonance. Furthermore, the dependence of the double-resonance

signal on microwave chopping frequency corresponded to a lifetime of roughly 10 msec for the initial sublevel.[5] One therefore concludes that the observed double-resonance spectra are associated with the longest decay time components, those in column 4 of Table I. Thus far, no double resonance correlated with the other decay components has been observed.

The distinguishing characteristics of the observed EPR[4] are summarized as follows: The resolved hyperfine interactions arise from two inequivalent fluorine nuclei whose internuclear axis lies approximately in a ⟨111⟩ direction. There is substantial anisotropy in the hfs, but not as much as for the corresponding V_k and H centers. The principal axes of the hfs and fine structure coincide, at least approximately. The fine structure is not axially symmetric. The magnitudes of the E parameter in the spin Hamiltonian are only slightly less than the magnitudes of the D parameter. The D and E values (in gauss) are, resepctively, +1552 and −590 for CaF_2, +1588 and −950 for SrF_2, and +1397 and −1160 for BaF_2. Specific directions to which the axes of the E term refer have not been specified thus far, primarily because magnetic-field-induced lifetime effects have limited the range over which angular dependences can be observed.

Since there are no close ⟨111⟩ fluoride pairs in the fluorite lattice, these facts imply that one of the two fluoride ions is in an interstitial position. But if this were the complete description, then the ⟨111⟩ internuclear axis would have three-fold symmetry, which would in turn require that $E=0$. Since the interstitial most certainly has very low mobility at these low temperatures, it is reasonable to conclude that the transient state is an STE morphology assumes the character of an incipient vacancy-interstitial pair.[4]

C. STE models

Figure 14(a) represents a $(1\bar{1}0)$ plane in the fluorite lattice, illustrating the ionic configuration of a self-trapped hole, or V_k center. As noted above, this cannot be the configuration of the STE observed by the double-resonance experiments. The three most probable STE morphologies are shown schematically in Fig. 14(b). The interstitial fluorine is at $F_{(2)}$. Fluoride sites labeled I, II, and III represent alternative locations of the vacancy which are qualitatively consistent with the EPR data. Site IV is included for completeness, although it maintains the three-fold ⟨111⟩ axis and is thus inconsistent with the large E term. Figure 14(b) comprises all morphologies for which the vacant site is a nearest neighbor

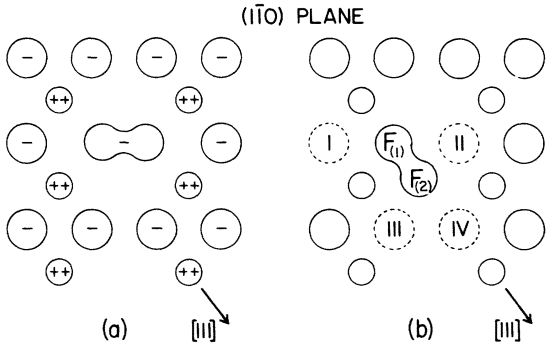

FIG. 14. Schematic representation of the self-trapped hole morphology in the fluorite lattice, as veiwed in the $(1\bar{1}0)$ plane, is shown in (a). Four proposed STE morphologies, discussed in the text, are shown in (b). The fluoride-ion sites labeled I–IV represent the possible near-neighbor sites for the vacancy accompanying generation of the interstitial fluoride ion which is bound in the molecular-ion pair $F_{(1)}$, $F_{(2)}$.

to either the interstitial site $F_{(2)}$ or the bound ion $F_{(1)}$.

The magnitudes of the parameter D in the spin Hamiltonian as well as the lifetimes are roughly comparable to those for the normal STE in NaF, KCl, RbCl, KBr, and RbBr.[15,16] This may be interpreted as implying that the electron distribution in the immediate vicinity of the ⟨111⟩-oriented F_2^- in fluorites is not drastically different from that near the ⟨110⟩ F_2^-, Cl_2^-, or Br_2^- in alkali halides. Thus the vacancy in the fluorites would appear to be quite near the F_2^- in order to produce the degree of departure from three-fold axial symmetry sufficient to account for the large E parameters. It is for this reason, as well as for simplicity, that we remove from consideration those morphologies for which the vacancy is more romote from the F_2^- than shown in Fig. 14(b). When the vacancy and interstitial are several nearest-neighbor distances apart, the lifetime against electron-hole recombination is very long, the exchange interaction is negligible, and the system has become a stable $F-H-$ center pair.

The three models I, II, and III each have C_{1h} point symmetry. Figure 15 shows schematically how the lowest electronic states of the STE correlate among C_{1h}, D_{2h}, and $D_{\infty h}$ symmetries, D_{2h} characterizing the normal STE in the NaCl-type lattice. The essential effects of the lower symmetry are to mix the singlet state B_{1u} with the triplet B_{2u}, and to mix the triplet B_{3u} with the pure triplet A_u, thereby lowering the radiative lifetime of A_u. This state, now the lowest A'', will remain the longest lived, however, and is certainly the initial state for the *microwave* tran-

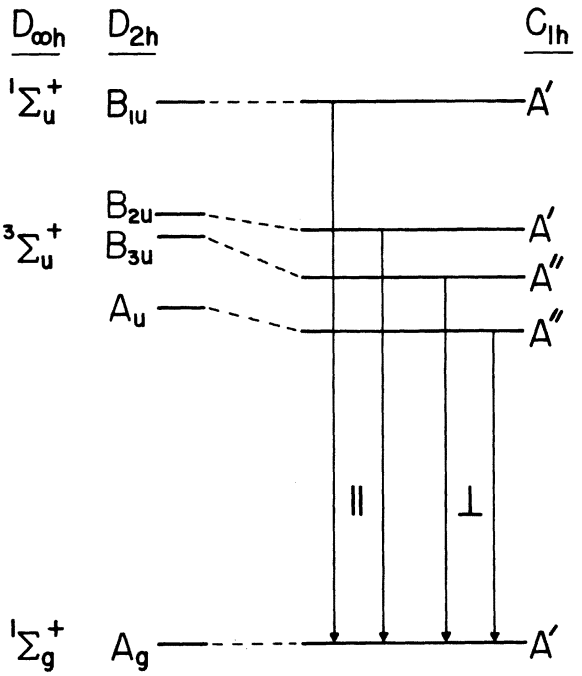

FIG. 15. Schematic representation of the lowest self-trapped exciton states is shown for environments having three different point symmetries. In $D_{\infty h}$ and D_{2h}, the principal symmetry axis is the axis connecting the relaxed pair of halide ions. In C_{1h}, the mirror plane (in the present case) is a {110} plane in the fluorite lattice, as in Fig. 14(b). The transitions marked ∥ are polarized in the mirror plane, and those marked ⊥ are polarized normal to the mirror plane.

sitions observed in the double-resonance experiment. Luminescent transitions from the A' states have electric dipole moments in the mirror plane $(1\bar{1}0)$, while transitions from the A'' states have moments perpendicular to the plane. In a later section we shall compare these transition moments with polarization measurements.

D. Origin of the lifetime components

At this stage there are two obvious explanations for the existence of the three principal lifetime components: They could originate in three different STE morphologies such as those of Fig. 14 or, alternatively, they could originate in the three triplet sublevels of one particular morphology. A combination of these two alternatives would also appear possible.

Let us consider a set of sublevels as in Fig. 15, supposing the set to arise from only one of the possible morphologies, say II. At sufficiently low temperature the relaxation time for transitions among these four sublevels will be longer than the radiative lifetime of any of them, and they will therefore behave as independent levels. Each will exhibit its own lifetime but, owing to the very small energy splittings, the decay components will not give observably different emission bands. This model appears to fit CaF_2 very well. The 8.8-msec component would correspond to the lowest A'' sublevel. However, the upper A' sublevel, essentially a singlet, would not seem to be populated to a significant extent: The 83-μsec component is more likely to arise from a triplet-singlet transition, and the weak 10-nsec component is not relevant since it gives a distinct emission spectrum.

The above model corresponds closely to behavior observed in the low-temperature emission of alkali iodides.[17] There is a slow, temperature-dependent decay component associated with the lowest sublevel and a second prominent component with shorter lifetime associated with one or both of the intermediate levels. The D parameter in the spin Hamiltonian is a factor of 30–40 larger for the alkali iodides than for the fluorites, although of the same sign. The difference is partly a result of the difference in spin-orbit coupling of fluorine and iodine. A decay component which can be ascribed to the singlet sublevel B_{1u} has not been observed in alkali halides, another feature in common with the present data. Since the lifetime of the lowest A'' sublevel in CaF_2 is approximately the same at 1.8 and 10 K, it probably represents the radiative lifetime for this recombination transition. The analogous transition in the alkali iodides is $A_u - A_g$ and is forbidden radiatively, even with spin-orbit coupling taken into account; this fact was used to explain the observed temperature dependence of the longest decay component.[17]

From the data of Fig. 11, it appears that the three levels having lifetimes τ_2, τ_3, and τ_4 at low temperature come into approximate thermal equilibrium at about 50 K. One can predict a lifetime

$$\tau = 3(\tau_2^{-1} + \tau_3^{-1} + \tau_4^{-1})^{-1} = 225\ \mu\text{sec}$$

in equilibrium if there are no other temperature-dependent effects. This is in satisfactory agreement with the data of Fig. 11; note that some further shortening of the lifetime is to be expected because of the observed thermal quenching of the luminescent intensity in this temperature range and because of possible vibrationally induced mixing of the singlet A' into the triplet states. Thus the observed τ at $T \approx 50$ K appears consistent with the quasiequilibrium model involving the three lower levels of Fig. 15. There is considerable thermal quenching as T approaches 300 K, and data are not adequate for quantitative lifetime

correlation there.

The measured lifetimes cannot be compared in any satisfying way to the triplet sublevel model without a detailed theory for the latter. Nevertheless, considering the lower symmetry of the fluorite STE, the lifetimes are of about the expected orders of magnitude relative to alkali-halide data. One might perhaps question the fact that τ_2 and τ_3 differ by a factor of 10, whereas the hole spin-orbit interaction, being screened from the crystal field, will produce comparable singlet-state admixtures in the middle A' and A'' states represented in Fig. 15. However, if the electron orbital is strongly affected by the low-symmetry crystal field, the dipole matrix elements with the two orthogonal π-like hole orbitals may well differ substantially. Consider also the fact that the E parameter of the spin Hamiltonian is comparable in magnitude to D. Prior work[4,16] indicates that magnetic dipole-dipole interaction between electron and hole is probably dominant in determining D and E for fluorites. If such is the case, the dipole-dipole interaction gives a contribution to D which is negative in the alkali chlorides and NaF but positive in the fluorites. This fact, as well as the observation that $|E|$ is comparable to $|D|$ in the fluorites (but not in the alkali halides), also suggests the large, nonaxial distortion of the electron orbital which the morphology II might be expected to produce and which would, in turn, cause a substantial difference in radiative lifetime between the middle A' and A'' states.

The data of Figs. 3 and 8 for CaF_2 are consistent with the triplet sublevel model, but those for SrF_2 appear contradictory because different decay components evidently give rise to different spectral components. In emission, the problem may be viewed as an additional, very weak band in the 300–450-nm range with a lifetime corresponding at least approximately to τ_4. The absorption spectra deviate more substantially, the behavior in Figs. 5 and 8 being describable approximately in terms of a band in the 2.5–3.0-eV range and another in the 3.1–3.6-eV range which decay together with roughly the lifetime τ_4. As a fraction of the total initial absorption, these bands comprise perhaps 0.08 or less. One suspects that the 2.5–3.0-eV absorption is, in fact, the F band. The F-center production efficiency measured in steady state at low temperature is much larger for SrF_2 than for CaF_2, and the inhomogeneously structured F band falls in just this spectral region. However, no complementary stable defect which absorbs around 3.3 eV has been reported.

These considerations suggest the following hypothesis: Suppose most of the long-lived absorption in the 2.5–3.5-eV range arises from a subsidiary vacancy-interstitial configuration, either one of those in Fig. 14(b) or a more remote F-H pair. Electron-hole recombination from this configuration gives rise to the weak, longer-wavelength emission, and this recombination process coincidentally exhibits a lifetime roughly the same as that of the longer component, τ_4, associated with the primary triplet state. This primary triplet would produce the majority of recombination luminescence and transient absorption in SrF_2 and would correspond to the STE state which dominates the CaF_2 data. It is possible that the subsidiary triplet state in SrF_2 is related to other lattice defects, which might account for the fact that the 3.3-eV band is well away from the expected F_2^- absorption.

The temperature dependence of emission decay times in SrF_2 (Fig. 12) can be interpreted in the above terms. Although most aspects of Fig. 12 are similar to the data for CaF_2 in Fig. 11, the longest time constant (τ_4) for SrF_2 persists to a considerably higher temperature. In fact τ_4, becomes *longer* above 22 K, until it finally drops sharply at still higher temperature. This apparent increase of the decay time with increasing temperature might be explained in terms of the extra component with $\tau \approx \tau_4$ which was hypothesized in the paragraph above. If the extra component has $\tau \approx 11$ msec and is weak at low temperature, then it might be difficult to distinguish from the component with $\tau_4 \approx 7.7$ msec arising from the primary triplet. However, if τ_4 begins to decrease near 22 K, as is observed in CaF_2, then the 11-msec component would become easily distinguished as the slowest. It is likely, furthermore, that the apparent increase of τ_3 at $T = 22$ K is due to the approach of the former 7.7-msec component to τ_3.

Thus the triplet sublevel model can be reconciled with the SrF_2 data, although not without some difficulty. As previously stated, one cannot rule out the alternative wherein different decay components in CaF_2 as well as SrF_2 actually arise from distinct morphologies. If this were the case there would be concern for questions such as why are not these decay components as well as distinct EPR spectra visible for each configuration and why do the different configurations give the same optical spectra, particularly in CaF_2. On balance, the triplet sublevel model would appear to be the more viable.

When account is taken of the semipermanent absorption for BaF_2, as discussed earlier, the results are reasonably consistent with the above comments. The experimental data for BaF_2 do not turn out to be crucial in determining the origin of the decay components. The near coincidence of the 3.4-eV absorption band in BaF_2 and the 3.3-

eV band in SrF_2 may suggest a common origin, even though the former is stable and the latter unstable at 10 K.

E. Luminescence polarization

Because the radiation employed in these and other experiments is of relatively high energy, principal precursors to the observed STE states are V_k centers, or self-trapped holes, and free electrons. Low-temperature irradiation can build up a concentration of V_k centers, and these can subsequently be aligned predominantly along a single $\langle 100 \rangle$ direction by illumination with linearly polarized light. It is appropriate to ask whether the models of Fig. 14 might be expected to produce a net polarization of luminescence when electrons are caused to recombine with aligned V_k centers.

With reference to Fig. 14, suppose V_k centers are aligned initially along [001]. If during recombination the STE were to retain the [001] F_2^- axis as it does in the alkali halides, the recombination luminescence from these triplet states would be expected to exhibit a net π polarization; i.e., the transition moment would lie in the (001) plane. The minimum motion of a [001] V_k center necessary to produce morphologies I and II is obvious: The hole need not exchange ions, and the motion is a combination of translation along [001] and rotation by approximately 55° around a $[1\bar{1}0]$ axis. For morphologies III and IV, the minimum motion requires that the hole hop to an adjacent location, retaining one of the original F^- ions. For this reason we consider I and II somewhat more likely to predominate.

Under the condition of minimum motion, it may be seen that [001] V_k centers can become STE morphologies I, II, and III lying in only two of the six $\{110\}$ planes, those two being $(1\bar{1}0)$ and $(\bar{1}10)$. Thus luminescent transitions of the type $A'' \rightarrow A'$ will have transition moments along $[1\bar{1}0]$ and $[\bar{1}10]$, giving the appearance of π-like polarization in the (001) plane. For $A' \rightarrow A'$ transitions, on the other hand, transition moments are in the planes $(1\bar{1}0)$ and $(\bar{1}10)$; the observed net polarization will be different for the three morphologies I, II, and III and can appear as either partial π-like or partial σ-like polarization. It is obvious that, for morphology IV, no particular $\langle 111 \rangle$ direction can be favored by prior $\langle 001 \rangle$ orientation, and thus no net polarization can result for this case.

According to Fig. 15, two of the three transitions which empty the triplet sublevels in morphologies I, II, and III are of the type $A'' \rightarrow A'$. Thus π-like polarization will dominate the observed luminescence if any of the following three conditions obtain: (i) Only the lowest level radiates, (ii) all three levels are in quasiequilibrium, or (iii) the three levels radiate roughly equal numbers of photons. Therefore, it appears that a net π polarization should be expected whether one assigns the different decay components to different sublevels or to different morphologies, including the simple [001] STE as well as those of Fig. 14(b).

At first sight this conclusion produces something of a dilemma, since net σ polarization of the recombination luminescence has in fact been measured for all three fluorites, using 0.1-mole% Tm-doped crystals.[1] However, continuing experiments on the polarization of STE luminescence in nominally pure crystals of CaF_2 and SrF_2 have yielded significantly different results, suggesting that impurities may in some circumstances have a determining influence on both magnitude and sign of the polarization of STE luminescence which is measured in these crystals. In experiments at both 77 and 10 K, the crystals were irradiated with x rays to produce a concentration of V_k centers sufficient to measure by optical absorption and to align along [001] with polarized ultraviolet light. Subsequent optical release of electrons from traps, or creation of conduction electrons by continuing low-intensity x-ray irradiation, produced emission corresponding approximately to the solid curves of Fig. 3. The emission in undoped CaF_2 was found to be π polarized with respect to the V_k alignment direction:

$$P = \frac{I_{\parallel} - I_{\perp}}{I_{\parallel} + I_{\perp}} = -0.05$$

after correction for dichroic absorption by the aligned V_k centers. Under optical stimulation of the recombination of trapped electrons and aligned V_k centers, undoped SrF_2 yielded σ-polarized emission ($P = 0.10$), though this polarization was weaker than that observed in the Tm-doped SrF_2. Under x-ray stimulation of the recombination of conduction electrons and oriented V_k centers in SrF_2, the polarization of the resulting luminescence dropped to $P \approx 0.02$. Although it is difficult to ascertain in this case what fraction of the recombination events involve oriented V_k centers, the results suggest that the luminescence may have intrinsically weaker σ polarization under x-ray production of recombination events.

Our tentative explanation of these results is as follows: In the initial irradiation electrons are trapped at impurities and at radiation-produced defects. Those complementary V_k centers which are very near the trapped electrons tend to survive subsequent continuing irradiation, since the Coulomb field of the V_k is largely screened by the close-trapped electron. If there are many extrinsic electron traps, as is the case in currently

available fluorites and certainly in the Tm-doped samples, then ultimately many of the V_k centers will be closely associated with close-trapped electrons. Although illumination will tend to excite all trapped electrons, close-pair emission may well predominate. On the other hand, conduction electrons produced by subsequent x-ray irradiation will avoid the close pairs and will instead tend to recombine with the isolated V_k centers. It is recombination at isolated V_k centers which would conform to the models discussed and which might be expected to be prevalent both in the present transient experiments and the EPR-optical double-resonance experiments. Close-pair, extrinsic recombination would be likely to predominate mainly in experiments involving direct optical excitation of electron traps. If one infers that such recombination exhibits a spectrum at least approximately congruent with that of intrinsic emission and furthermore shows a net σ polarization, the variability of emission polarization with sample and excitation method can be explained.

An indication that V_k centers are, in fact, distributed preferentially near Tm^{2+} sites after prolonged x-ray irradiation of thulium-doped fluorite crystals has been obtained from kinetics of V_k motion.[1,9] On the other hand, electron-nuclear double-resonance measurements on the V_k ground state have not shown any influence of nearby Tm^{2+} ions.[18] However, the interaction we are considering, which is between a STE and a Tm^{3+}, is not inconsistent with the electron-nuclear double-resonance data. The situation may be analogous to that found in $KCl:Ag^+$ and $KCl:Tl^+$ by Delbecq, Toyozawa, and Yuster,[19] where recombination luminescence due to tunneling between V_k centers and close impurity atoms is σ polarized with respect to orientation of the V_k axis, although the comparable *intrinsic* luminescence in KCl is π polarized. A plausible mechanism in the present case might be that the field of the impurity ion mixes enough of the singlet level (upper A' in Fig. 15) into the triplet levels to dominate the transition. The decay time $\tau < 40$ nsec observed for photostimulated recombination luminescence,[1] and possibly the 10-nsec component of luminescence observed in the present experiment, may be characteristic of such close-pair recombination events.

V. SUMMARY

Considering the results of the present study in conjunction with previous work, particularly Refs. 1 and 4, the following general conclusions are drawn:

(i) The intrinsic recombination luminescence in CaF_2, SrF_2, and BaF_2 originates principally in long-lived triplet states of the self-trapped exciton. In CaF_2 and SrF_2, on which the more detailed observations were made, the luminescence comprises three main decay-time components at low temperature. The three components have approximately equal time-integrated intensities, and the emitting levels appear to come into thermal equilibrium at a temperature of about 50 K.

(ii) Optical transitions from these same metastable states to higher STE states account for transient absorption bands observed in the ultraviolet and visible spectral ranges following a pulse of ionizing radiation. Qualitatively, the transient absorption spectra resemble STE spectra found in the alkali halides.[6,7] Modeling of the transitions, e.g., as analogs in certain respects of F- and V_k- or H-center transitions, can be carried over from the alkali-halide studies, as can the characterization of parameters such as optical binding energies. The ordinary color-center bands (e.g., F, H, and V_k bands) which are produced in this experiment are quite small relative to the STE bands.

(iii) Microwave-optical double-resonance experiments in fluorites by Call *et al.*[4] have established that the resolved hyperfine interactions in the STE arise from two inequivalent fluorine nuclei whose internuclear axis lies approximately in a $\langle 111 \rangle$ direction, in contrast to the self-trapped hole involving two equivalent fluorine nuclei along $\langle 100 \rangle$. It was suggested in that work that the STE configuration in fluorites resembles a nearest-neighbor F-H-center pair. In the present paper we have elaborated somewhat on the possible configurations of this type. At present, the time-resolved data do not distinguish with certainty between models which attribute the three observed decay-time components to lifetime-resolved triplet sublevels belonging to the same local ionic configuration, or to three different local ionic configurations. The data for CaF_2, and many of the observations on SrF_2, appear to be most readily accommodated within the triplet-sublevel model. Certain spectrally distinct long-lived components of emission and absorption in SrF_2 may, however, imply that at least two distinct ionic configurations occur upon exciton relaxation. Comparison of the predicted polarization properties with experiment appears to be complicated by impurity effects, but can be accounted for in a way generally consistent with our suggested picture of the STE.

ACKNOWLEDGMENTS

We wish to thank P. J. Call and I. B. Owen for communication of unpublished results, and J. W. Williams for experimental assistance.

[1]J. H. Beaumont, W. Hayes, D. L. Kirk, and G. P. Summers, Proc. R. Soc. A 315, 69 (1970).
[2]M. N. Kabler, in *Point Defects in Solids*, edited by J. H. Crawford and L. M. Slifkin (Plenum, New York, 1972), Vol. 1, Chap. 6.
[3]W. Hayes and J. W. Twidell, Proc. Phys. Soc. Lond. 79, 1295 (1962); J. H. Beaumont, W. Hayes, G. P. Summers, and J. W. Twidell, Solid State Commun. 6, 903 (1968).
[4]P. J. Call, W. Hayes, and M. N. Kabler, J. Phys. C 8, L60 (1975).
[5]P. J. Call (private communication).
[6]R. G. Fuller, R. T. Williams, and M. N. Kabler, Phys. Rev. Lett. 25, 446 (1970).
[7]R. T. Williams and M. N. Kabler, Phys. Rev. B 9, 1897 (1974).
[8]D. A. Patterson and R. G. Fuller, Phys. Rev. Lett. 18, 1123 (1967).
[9]W. Hayes and A. M. Stoneham, in *Crystals with the Fluorite Structure*, edited by W. Hayes (Oxford U. P., London, 1974), Chap. 4.
[10]D. Pooley, Solid State Commun. 3, 241 (1965); F. J. Keller and F. W. Patten, Solid State Commun. 7, 1603 (1969); M. N. Kabler, in *Radiation Damage Processes in Materials*, edited by C. H. S. Dupuy (Noordhoff, Leyden, 1975), p. 171.
[11]R. T. Williams, R. G. Fuller, M. N. Kabler, and V. H. Ritz, Rev. Sci. Instrum. 40, 1361 (1969).
[12]W. Hayes and R. F. Lambourn, Phys. Status Solidi B 57, 693 (1973).
[13]W. Hayes, R. F. Lambourn, and J. P. Stott, J. Phys. C 7, 2429 (1974).
[14]B. C. Cavenett, W. Hayes, I. C. Hunter, and A. M. Stoneham, Proc. Phys. Soc. Lond. A 309, 53 (1969).
[15]M. J. Marrone, F. W. Patten, and M. N. Kabler, Phys. Rev. Lett. 31, 467 (1973).
[16]P. J. Call, W. Hayes, R. Hazimura, and M. N. Kabler, J. Phys. C 8, L56 (1975).
[17]J. U. Fischbach, D. Frohlich, and M. N. Kabler, J. Lumin. 6, 29 (1973).
[18]R. F. Marzke and R. L. Mieher, Phys. Rev. 182, 453 (1969).
[19]C. J. Delbecq, Y. Toyozawa, and P. H. Yuster, Phys. Rev. B 9, 4497 (1974).